Alexandria Engineering Journal (2014) 53, 769–778

HOSTED BY

ELSEVIER

Alexandria University

Alexandria Engineering Journal

www.elsevier.com/locate/aej
www.sciencedirect.com

ORIGINAL ARTICLE

Numerical study of entropy generation for forced convection flow and heat transfer of a Jeffrey fluid over a stretching sheet

Nemat Dalir *

Department of Mechanical Engineering, Salmas Branch, Islamic Azad University, Salmas, Iran

Received 19 February 2014; revised 8 July 2014; accepted 21 August 2014
Available online 22 September 2014

KEYWORDS

Jeffrey fluid;
Linearly stretching sheet;
Keller's box method;
Entropy generation

Abstract Entropy generation for the steady two-dimensional laminar forced convection flow and heat transfer of an incompressible Jeffrey non-Newtonian fluid over a linearly stretching, impermeable and isothermal sheet is numerically investigated. The governing differential equations of continuity, momentum and energy are transformed using suitable similarity transformations to two nonlinear coupled ordinary differential equations (ODEs). Then the ODEs are solved by applying the numerical implicit Keller's box method. The effects of various parameters of the flow and heat transfer including Deborah number, ratio of relaxation to retardation times, Prandtl number, Eckert number, Reynolds number and Brinkman number on dimensionless velocity, temperature and entropy generation number profiles are analyzed. The results reveal that the entropy generation number increases with the increase of Deborah number while the increase of ratio of relaxation to retardation times causes the entropy generation number to reduce. A comparative study of the numerical results with the results from an exact solution for the dimensionless velocity gradient at the sheet surface is also performed. The comparison shows excellent agreement within 0.05% error.

1. Introduction

During the last few decades, researchers have shown much interest in the flows of non-Newtonian fluids. The reason for such accelerating interest is in fact due to the wide range of applications of non-Newtonian fluids. The non-Newtonian fluids have applications in various areas such as in chemical and petroleum industries, geophysics and biological sciences. The flows of non-Newtonian fluids have governing equations which are more complex than the Navier–Stokes equations. The governing equations for flows of non-Newtonian fluids are in fact the consequence of the constitutive relations which are used to predict the rheological behavior of these fluids. Due to versatile nature of the non-Newtonian fluids, various constitutive relations have been considered in the literature. One of the various constitutive relations used for non-Newtonian fluids is the Jeffrey fluid model. The Jeffrey fluid model is a linear

* Tel.: +98 937 612 1607.
E-mail address: dalir@aut.ac.ir.
Peer review under responsibility of Faculty of Engineering, Alexandria University.

http://dx.doi.org/10.1016/j.aej.2014.08.005

Nomenclature

a	stretching rate (s^{-1})
Br	Brinkman number ($=\mu\cdot(u_w)^2/k\cdot\Delta T$) (–)
$C_{f,x}$	local skin friction coefficient ($=(1+\beta)f''(0)/(1+\lambda)Re_x^{0.5}$) (–)
C_p	specific heat at constant pressure of the fluid ($J\,kg^{-1}\,K^{-1}$)
Ec	Eckert number ($=(u_w)^2/C_p(T_w-T_\infty)$) (–)
f	dimensionless velocity variable ($=-v/(av)^{0.5}$) (–)
k	thermal conductivity ($W\,m^{-1}\,K^{-1}$)
m	power of exact solution in Eq. (12) (–)
Nu_x	local Nusselt number ($=-\theta'(0)/Re_x^{-0.5}$) (–)
N_S	entropy generation number (–)
Pr	Prandtl number ($=\mu C_p/k$) (–)
Re_x	local Reynolds number ($=u_w x/\upsilon$) (–)
S_{gen}	local volumetric entropy generation rate ($W\,m^{-3}\,K^{-1}$)
$(S_{gen})_0$	characteristic entropy generation rate ($W\,m^{-3}\,K^{-1}$)
T	temperature variable (K)
T_w	given temperature of the sheet (K)
T_∞	temperature of fluid far away from the sheet (K)
ΔT	sheet and free-stream temperature difference ($=T_w-T_\infty$) (K)
u	velocity in x-direction ($m\,s^{-1}$)
u_w	velocity of the sheet ($m\,s^{-1}$)
v	velocity in y-direction ($m\,s^{-1}$)
x	horizontal coordinate (m)
y	vertical coordinate (m)

Greek symbols

α	thermal diffusivity ($m^2\,s^{-1}$)
β	Deborah number ($=a\lambda_1$) (–)
η	similarity variable ($=y(a/\upsilon)^{0.5}$) (–)
θ	dimensionless temperature variable ($=T-T_\infty/T_w-T_\infty$) (–)
λ	ratio of relaxation to retardation times (–)
λ_1	relaxation time (s)
μ	dynamic viscosity ($N\,s\,m^{-2}$)
υ	kinematic viscosity ($m^2\,s^{-1}$)
ρ	density ($kg\,m^{-3}$)
ψ	stream function ($m^2\,s^{-1}$)
Ω	dimensionless temperature difference ($=\Delta T/T_\infty$) (–)

Subscripts

∞	infinity
f	fluid
w	sheet surface

model which uses time derivatives instead of convected derivatives which are used for example in the Maxwell fluid model.

The area of non-Newtonian fluid flow and heat transfer has been given much attention in the last few years. For instance, Molla and Yao [1] investigated mixed convection heat transfer of non-Newtonian fluids over a flat plate using a modified power-law viscosity model. They solved the boundary layer equations by marching from the leading edge downstream and presented the numerical results for a shear-thinning fluid in terms of velocity and temperature distribution. Hayat et al. [2] studied the magneto-hydrodynamic (MHD) flow of a Jeffery fluid in a porous channel. They constructed series solutions to the nonlinear problem by using the homotopy analysis method (HAM). Sahoo [3] considered the flow and heat transfer of a non-Newtonian third grade fluid due to a linearly stretching plate with partial slip. He adopted a second order numerical scheme to solve the differential equations and obtained the combined effects of the partial slip and the third grade fluid parameter on velocity and temperature fields. Prasad et al. [4] considered the steady viscous incompressible two-dimensional MHD flow of an electrically conducting power law fluid over a vertical stretching sheet. They assumed the stretching of surface velocity and the prescribed surface temperature to vary linearly with the distance from the slit and solved the boundary layer equations by Keller's box method. Hayat et al. [5] investigated the three-dimensional flow of Jeffrey fluid over a linearly stretching surface and solved the nonlinear coupled system of governing equations using a homotopy analysis method. Hayat et al. [6] studied the unsteady boundary layer flow and heat transfer of an incompressible Jeffrey fluid over a linearly stretching sheet. They obtained the analytical solutions of the arising differential system by homotopy analysis technique. Khan et al. [7] presented a mathematical model for unsteady stagnation point flow of a linear viscoelastic fluid bounded by a stretching/shrinking sheet. They solved the resulting nonlinear problems by a homotopy analysis approach. Malik et al. [8] considered the Jeffrey fluid flow with a pressure-dependent viscosity. They numerically solved two types of flow problem, namely, Poiseulle flow and Couette flow for the Jeffrey fluid. Hayat et al. [9] examined the flow and heat transfer of an incompressible Jeffery fluid over a stretching surface with power law heat flux and heat source in the presence of thermal radiation. They developed homotopic solutions for velocity and temperature fields. Hayat et al. [10] investigated the boundary layer stretched flow and heat transfer of a Jeffrey fluid subject to convective boundary conditions. They solved the governing dimensionless equations by using the homotopy analysis approach. They analyzed the influence of embedded parameters and found that the temperature is an increasing function of the Biot number. Turkyilmazoglu and Pop [11] investigated the flow and heat transfer of a Jeffrey fluid near the stagnation point over a stretching/shrinking sheet with a parallel external flow. They indicated that structure of the analytical solutions strongly depends on a parameter measuring the ratio of strength of the external flow to surface stretching/shrinking. Goyal and Bhargava [12] analyzed the effect of velocity slip on the MHD flow and heat transfer of non-Newtonian nanofluid over a stretching sheet with a heat source/sink. They also considered the Brownian motion and thermophoresis effects and solved the differential equations by the variational finite element method. Qasim [13] studied the combined effects of heat and mass transfer in Jeffrey fluid over a stretching sheet in the presence of heat source/sink.

They derived exact solutions by power series method using Kummer's confluent hyper-geometric functions and examined the effects of emerging parameters on velocity, temperature and concentration profiles. Nadeem et al. [14] numerically studied the steady 2-D flow of a Jeffrey fluid over a linearly stretching sheet in the presence of nanoparticles.

In the last decade, many researchers have studied the entropy generation in fluid flow and heat transfer over surfaces. Aiboud and Saouli [15] presented the application of second law analysis of thermodynamics to viscoelastic magneto-hydrodynamic (MHD) flow over a stretching surface. They analytically obtained the velocity and temperature profiles using the Kummer's functions and computed the entropy generation number. Makinde [16] analyzed the inherent irreversibility in hydromagnetic boundary layer flow of variable viscosity fluid over a semi-infinite flat plate under the influence of thermal radiation and Newtonian heating. Using local similarity solution technique and shooting quadrature, he numerically obtained the velocity, temperature and entropy generation number. Dehsara et al. [17] numerically analyzed entropy generation for the magneto-hydrodynamic (MHD) mixed convection flow over a nonlinear stretching inclined transparent plate embedded in a porous medium due to solar radiation. Butt et al. [18] discussed the boundary layer flow and heat transfer analysis of a second grade fluid over a stretching sheet through a porous medium and investigated the effect of viscoelasticity on entropy generation using the Homotopy analysis method (HAM). Butt et al. [19] reported the effects of velocity slip on entropy generation in the boundary layer flow over a vertical surface with convective boundary condition. They numerically solved the governing equations using the shooting method and presented expressions for the entropy generation number and Bejan number. Malvandi et al. [20] analytically studied the steady two-dimensional boundary layer flow over an isothermal flat plate by homotopy perturbation method (HPM) and analyzed the entropy generation inside the boundary layer. Galanis and Rashidi [21] studied the entropy generation in non-Newtonian fluids due to heat transfer in entrance region of ducts. Butt et al. [22] made an investigation on entropy generation within a steady laminar mixed convective MHD flow of a viscoelastic fluid over a stretching sheet. They solved the governing equations using the homotopy analysis method and obtained expressions for local entropy generation number, Bejan number, and average Bejan number. Butt and Ali [23] analyzed the effects of entropy generation in MHD flow over a permeable stretching sheet embedded in a porous medium in the presence of viscous dissipation. They obtained analytical solutions of momentum and energy equations in terms of Kummer's functions and computed the entropy generation number and Bejan number. Noghrehabadi et al. [24] analyzed the boundary layer heat transfer and entropy generation of a nanofluid over an isothermal linearly stretching sheet with heat generation/absorption. They took into account the development of nanoparticles concentration gradient due to slip and the effects of Brownian motion and thermophoresis. Dehsara et al. [25] investigated the entropy generation of MHD mixed convection flow of nanofluid over a nonlinear stretching inclined transparent plate embedded in a porous medium. Using a numerical algorithm, they solved the governing equations, in the presence of the effects of viscous dissipation, variable magnetic field and solar radiation. More literature survey makes it clear that the entropy generation has not been investigated for the flow and heat transfer of a Jeffrey non-Newtonian fluid over a stretching surface.

The purpose of the present study was to venture further in the area of entropy generation for the steady two-dimensional laminar flow of a Jeffrey fluid over a linearly stretching sheet. To the best of the author's knowledge, the investigation of entropy generation for the steady flow of Jeffrey fluid over a linearly stretching sheet is presented for the first time in the present study. The boundary layer flow and heat transfer equations are transformed using the similarity transformations to a system of two nonlinear ordinary differential equations which are then solved by using Keller's box method. Various profiles of dimensionless velocity, temperature and entropy generation number are plotted and the effects of various parameters such as Deborah number, ratio of relaxation to retardation times, Prandtl number, Reynolds number and Brinkman number on velocity, temperature and entropy generation number are analyzed.

2. Mathematical formulation

The steady two-dimensional laminar flow of a non-Newtonian fluid over a flat horizontal sheet is considered. The non-Newtonian fluid is considered to be an incompressible viscous Jeffrey fluid. The sheet is assumed to be linearly stretching, isothermal and impermeable. The viscous dissipation effect is also taken into consideration. The governing equations including mass, momentum and energy conservations are as follows:

$$\frac{\partial u}{\partial x}+\frac{\partial v}{\partial y}=0 \tag{1}$$

$$u\frac{\partial u}{\partial x}+v\frac{\partial u}{\partial y}=\frac{\upsilon}{(1+\lambda)}\times\left[\frac{\partial^2 u}{\partial y^2}+\lambda_1\left(u\frac{\partial^3 u}{\partial x\partial y^2}-\frac{\partial u}{\partial x}\frac{\partial^2 u}{\partial y^2}+\frac{\partial u}{\partial y}\frac{\partial^2 u}{\partial x\partial y}+v\frac{\partial^3 u}{\partial y^3}\right)\right] \tag{2}$$

$$u\frac{\partial T}{\partial x}+v\frac{\partial T}{\partial y}=\alpha\frac{\partial^2 T}{\partial y^2}+\frac{\upsilon}{C_p(1+\lambda)}\times\left[\left(\frac{\partial u}{\partial y}\right)^2+\lambda_1\left(u\frac{\partial u}{\partial y}\frac{\partial^2 u}{\partial x\partial y}+v\frac{\partial u}{\partial y}\frac{\partial^2 u}{\partial y^2}\right)\right] \tag{3}$$

where u and v are the velocity components in x and y directions respectively, υ is the kinematic viscosity of the fluid, α is the thermal diffusivity of the fluid, C_p is the specific heat at constant pressure of the fluid, λ is the ratio of relaxation to retardation times, and λ_1 is the relaxation time. The boundary conditions are as follows:

$$\begin{aligned} &u=u_w(x)=ax,\ v=0,\ T=T_w \text{ at } y=0\\ &u\to 0,\ \tfrac{\partial u}{\partial y}\to 0,\ T\to T_\infty \text{ as } y\to\infty \end{aligned} \tag{4}$$

where u_w is the velocity by which the sheet is being stretched, a is the stretching rate of sheet which is a constant with dimension of $(\text{time})^{-1}$, and finally T_w and T_∞ are the temperature of isothermal sheet and the free-stream temperature respectively.

The following similarity transformations are used to transform the boundary layer flow and heat transfer equations to nonlinear ODEs:

$$\eta = y\left(\frac{a}{\upsilon}\right)^{0.5}, f(\eta) = \frac{-v}{(a\upsilon)^{0.5}}, f'(\eta) = \frac{u}{ax}, \theta(\eta) = \frac{T - T_\infty}{T_w - T_\infty} \quad (5)$$

where η and f are the similarity variable and the dimensionless stream-function respectively. f' and θ are the dimensionless velocity and dimensionless temperature as well. The continuity equation is directly satisfied as:

$$u = \frac{\partial \psi}{\partial y}, v = -\frac{\partial \psi}{\partial x} \quad (6)$$

where ψ is the stream-function. Using the similarity transformations of Eq. (6), Eqs. (1)–(3) are transformed to:

$$f''' + (1+\lambda)(ff'' - f'^2) + \beta(f''^2 - ff'''') = 0 \quad (7)$$

$$\theta'' + \mathrm{Pr} f\theta' + \frac{\mathrm{Pr} \cdot Ec}{(1+\lambda)}\left[f''^2 + \beta\left(f'f''^2 - ff''f''''\right)\right] = 0 \quad (8)$$

where $\beta = a\lambda_1$ is Deborah number, $Pr = \mu C_p/k$ is Prandtl number and $Ec = (u_w)^2/C_p(T_w - T_\infty)$ is the Eckert number. The transformed boundary conditions are as follows:

$$\begin{aligned} &f(0) = 0, f'(0) = 1, \theta(0) = 1 \\ &f'(\infty) = 0, f''(\infty) = 0, \theta(\infty) = 0 \end{aligned} \quad (9)$$

The parameters of engineering interest are the local skin friction coefficient and the local Nusselt number, which are defined as follows:

$$C_{f,x} = \frac{1+\beta}{1+\lambda}\frac{f''(0)}{Re_x^{0.5}} \quad (10)$$

$$Nu_x = -\frac{\theta'(0)}{Re_x^{-0.5}} \quad (11)$$

where $Re_x = u_w{\cdot}x/\upsilon$ is the local Reynolds number. The exact solution for the dimensionless velocity, using Eq. (7) with boundary conditions of Eq. (9), is as follows [6]:

$$f(\eta) = \frac{1 - e^{-m\eta}}{m}, m = \left(\frac{1+\lambda}{1+\beta}\right)^{0.5} \quad (12)$$

where the second derivative of the exact solution for dimensionless velocity is $f''(\eta) = -me^{-m\eta}$ which gives the dimensionless velocity gradient at the sheet surface using the exact solution to be $f''(0)\_exact = -m$.

3. Entropy generation analysis

The local entropy generation rate per unit volume for the Jeffrey fluid is as follows:

$$S_{gen} = \frac{k}{T_\infty^2}\left(\frac{\partial T}{\partial y}\right)^2 + \frac{\mu}{T_\infty(1+\lambda)} \times \left[\left(\frac{\partial u}{\partial y}\right)^2 + \lambda_1\left(u\frac{\partial u}{\partial y}\frac{\partial^2 u}{\partial x \partial y} + v\frac{\partial u}{\partial y}\frac{\partial^2 u}{\partial y^2}\right)\right] \quad (13)$$

where the first term on the right-hand side of Eq. (13) is the entropy generation due to heat transfer, and the second term is the entropy generation due to viscous dissipation and Jeffrey fluid effect. In order to define the dimensionless entropy generation number, a characteristic entropy generation rate $(S_{gen})_0$ is defined as follows:

$$(S_{gen})_0 = \frac{k}{T_\infty^2}\frac{(\Delta T)^2}{x^2} \quad (14)$$

Thus, the dimensionless entropy generation number is defined as the ratio of local volumetric entropy generation rate to the characteristic entropy generation rate:

$$N_S = \frac{S_{gen}}{(S_{gen})_0} \quad (15)$$

Therefore, the dimensionless entropy generation number is obtained as follows:

$$N_S = Re \cdot \theta'^2 + \frac{Br \cdot Re}{\Omega(1+\lambda)} \cdot \left[f''^2 + \beta\left(f'f''^2 - ff''f''''\right)\right] \quad (16)$$

where Re, Br and Ω are the Reynolds number, the Brinkman number and the dimensionless temperature difference which are defined as:

$$Re = \frac{u_w \cdot x}{\upsilon}, Br = \frac{\mu \cdot (u_w)^2}{k \cdot \Delta T}, \Omega = \frac{\Delta T}{T_\infty} \quad (17)$$

4. Numerical method of solution

The numerical finite-difference implicit Keller's box method is used to solve Eqs. (7) and (8) with the boundary conditions of Eq. (9). To apply the method, the nonlinear ODEs (7-8) are first transformed to a system of first order ODEs. Then, using backward finite differences, the difference equations are obtained. In order to linearize the problem, the Newton's method of linearization is employed [26]. Afterward, by the use of a block-three diagonal matrix algorithm, the system of linearized difference equations is iteratively solved. The step size of $\Delta\eta = 0.05$ and the convergence criterion of 10^{-4} is applied to take into account the boundary layer effect.

5. Results and discussion

Boundary layer flow and heat transfer of a Jeffrey fluid over a linearly stretching sheet is considered. The governing equations are transformed to two nonlinear ODEs and then solved using a numerical implicit finite-difference Keller's box algorithm. Table 1 compares values of dimensionless velocity gradient of fluid at the sheet surface $f''(0)$ using the numerical solution of the present paper with the exact solution [6] for various values of the physical parameters β and λ. It is seen that the numerical values of $f''(0)$ are in excellent agreement within a relative error of 0.05% with the ones from the exact solution of Eq. (12). It is also observed that $f''(0)$ increases with the increase of Deborah number β for a constant value of λ. It may also be seen that, at the constant value of $\beta = 0.2$, the dimensionless velocity gradient at sheet surface $f''(0)$ reduces with an increase in the ratio of relaxation to retardation times λ.

Table 2 shows the values of dimensionless local skin friction group $C_{f,x}Re_x^{0.5}$ for various values of physical parameters β and λ using Eq. (10) and the numerical values of $f''(0)$ from Table 1. For a constant β, it can be observed that $C_{f,x}\ Re_x^{0.5}$ increases with the increase of λ. With the increase of the ratio of relaxation to retardation time λ, due to the augmentation of relaxation duration of the non-Newtonian fluid, the velocity of the fluid near the sheet surface declines. Hence the thickness of hydrodynamic boundary layer increases which causes the local skin friction coefficient to increase. It is also observable that, at a constant λ, $C_{f,x}\ Re_x^{0.5}$ reduces with increase of β. The reason is that the increase of the Deborah number β leads to a higher

Table 1 Values of $f''(0)$ for various values of the physical parameters using the present numerical solution and the exact solution [6].

$f''(0)$ for various β: $\lambda = 0.2$			$f''(0)$ for various λ: $\beta = 0.2$		
β	$f''(0)$	$f''(0)$_exact	λ	$f''(0)$	$f''(0)$_exact
0.0	−1.09641580	−1.09544512	0.0	−0.91468190	−0.91287093
0.2	−1.00124052	−1.00000000	0.2	−1.00124052	−1.00000000
0.4	−0.92724220	−0.92582010	0.4	−1.08100090	−1.08012345
0.6	−0.86755715	−0.86602540	0.6	−1.15533663	−1.15470054
0.8	−0.81808091	−0.81649658	0.8	−1.22521512	−1.22474487
1.0	−0.77618697	−0.77459667	1.0	−1.29134772	−1.29099445
1.2	−0.74010502	−0.73854895	1.2	−1.35427540	−1.35400640
1.4	−0.70859214	−0.70710678	1.4	−1.41442077	−1.41421356
1.6	−0.68074654	−0.67936622	1.6	−1.47212137	−1.47196014
1.8	−0.65589608	−0.65465367	1.8	−1.52765178	−1.52752523
2.0	−0.63352833	−0.63245553	2.0	−1.58123895	−1.58113883
2.2	−0.61324514	−0.61237244	2.2	−1.63307294	−1.63299316
2.4	−0.59473195	−0.59408853	2.4	−1.68331479	−1.68325082
2.6	−0.57773665	−0.57735027	2.6	−1.73210240	−1.73205081
2.8	−0.56205463	−0.56195149	2.8	−1.77955488	−1.77951304
3.0	−0.54751791	−0.54772256	3.0	−1.82577595	−1.82574186
3.2	−0.53398720	−0.53452248	3.2	−1.87085660	−1.87082869
3.4	−0.52134592	−0.52223297	3.4	−1.91487716	−1.91485422
3.6	−0.50949569	−0.51075392	3.6	−1.95790896	−1.95789002
3.8	−0.49835287	−0.50000000	3.8	−2.00001569	−2.00000000
4.0	−0.48784584	−0.48989795	4.0	−2.04125449	−2.04124145

motion of fluid particles inside the boundary layer, especially in the vicinity of the sheet surface. Thus the velocity boundary layer thickness lessens which results in lower values of skin friction coefficient.

Table 3 presents the numerical values of dimensionless local Nusselt group $-\theta'(0) = Nu_x\, Re_x^{-0.5}$ for various values of the physical parameters λ, β, Pr and Ec. It can be seen that, in the case of the absence of viscous dissipation (i.e. $Ec = 0$), $Nu_x\, Re_x^{-0.5}$ decreases for the higher values of λ. Nevertheless, for a nonzero Eckert number, $Nu_x\, Re_x^{-0.5}$ increases with the increase of λ. This different trend of variation for the Nusselt number with λ can be attributed to the thermal boundary layer thickness. In the case of the absence of viscous dissipation (i.e. $Ec = 0$), the increase of ratio of relaxation to retardation times λ adds to the thickness of thermal boundary layer, and, as a result, the Nusselt number reduces. However, in the case of the presence of viscous dissipation, the increase of thermal boundary layer thickness due to increase of λ cannot overcome the reduction of boundary layer thickness caused by viscous dissipation. Thus the thickness of the thermal boundary layer reduces and consequently the dimensionless Nusselt group rises. The variation of $Nu_x\, Re_x^{-0.5}$ with Deborah number β is observed to be exactly opposite of that of λ. The Nu increases with the increase of β in no-viscous-dissipation case (i.e. $Ec = 0$) while it reduces with increase of β in viscous-dissipation-present case (i.e. $Ec > 0$). The dimensionless Nusselt group $Nu_x\, Re_x^{-0.5}$ is also observed to augment with the increase of Prandtl number when $Ec = 0$, but it is decreased with a rise in Pr when $Ec > 0$. It is finally seen that the increase of Ec causes $Nu_x\, Re_x^{-0.5}$ to quickly diminish when the other physical parameters are kept constant.

Fig. 1 shows the variation of the dimensionless velocity gradient at the sheet surface $f''(0)$ with the Deborah number β for $\lambda = 0.2$. The solid line indicates the numerical solution of the present study while the black circles indicate the exact solution (i.e. Eq. (12)). It is seen that an excellent agreement between the numerical solution of the present study and the exact solution is obtained. It can also be seen that $f''(0)$ increases with the increase of the Deborah number β. The variation of $f''(0)$ with the ratio of relaxation to retardation times λ is demonstrated in Fig. 2 for $\beta = 0.2$. Here again a very good agreement is observed between the numerical and exact solutions. It is also revealed that the fluid dimensionless velocity at the sheet surface $f''(0)$ reduces with the increase of λ.

Fig. 3 shows the dimensionless velocity profiles $f'(\eta)$ for various values of the Deborah number β for $\lambda = 0.2$. It can be observed that the increase of the Deborah number β causes the fluid velocity inside the boundary layer to increase. Since the Deborah number is proportional to the stretching rate of the sheet ($\beta = a\lambda_1$), the increase of Deborah number results in a higher fluid motion in the boundary layer especially adjacent the surface of sheet. This higher fluid motion increases the thickness of the hydrodynamic boundary layer and consequently raises the fluid velocity. Fig. 4 illustrates the dimensionless velocity profiles $f'(\eta)$ for several values of λ when $\beta = 0.2$. It is seen that the increase of λ causes the reduction of boundary layer velocity of fluid. The physical parameter λ is inversely proportional to the retardation time of the non-Newtonian fluid. Hence, an increase in λ means a decrease in fluid retardation time which in effect prevents the hastening of fluid motion. As a result, the thickness of velocity boundary layer diminishes and the velocity of the fluid is increased.

Fig. 5 shows the dimensionless temperature profiles $\theta(\eta)$ for various values of the Deborah number β for $\lambda = 0.2$, $Ec = 1.0$, $Pr = 1.0$. It is observable that, in the vicinity of the sheet surface, the temperature slightly boosts with the increase of β. However, it can be said the Deborah number β does not have much effect on the temperature at some distance from the sheet inside the boundary layer. The increase of temperature by an increase in β in sheet surface vicinity

Table 2 Numerical values of $C_{f,x}\ Re_x^{0.5}$ for various values of the physical parameters.

β	λ	$C_{f,x}\ Re_x^{0.5}$
0	0.0	−1.00147175
	0.6	−0.79086006
	1.2	−0.67428162
	1.8	−0.59764222
0.5	0.0	−1.22786453
	0.6	−0.96901469
	1.2	−0.82598351
	1.8	−0.73203014
2.0	0.0	−1.73569391
	0.6	−1.37082453
	1.2	−1.16846343
	1.8	−1.03546901

may be a reason of vaster motions of the fluid particles which in effect thicken the thermal boundary layer. These motions result in a slight temperature increase for fluid near the sheet surface because the highest temperature difference between the free-stream and the boundary layer occurs at the sheet surface. However, further from the sheet surface inside the boundary layer, there is not much temperature difference for the fluid in a point inside the boundary layer and another point outside the boundary layer. Thus the increased motion of fluid particles does not considerably affect the thermal boundary layer thickness further from the sheet surface, and as a result the temperature does not noticeably vary. The dimensionless temperature profiles for various values of λ when $\beta = 0.2$, $Ec = 1.0$, $Pr = 1.0$ are demonstrated in Fig. 6. The fluid

Table 3 Numerical values of $-\theta'(0) = Nu_x\ Re_x^{-0.5}$ for various values of the physical parameters.

Pr	β	λ	$Ec = 0.0$	$Ec = 1.0$	$Ec = 3.0$
1.0	0	0.0	0.58750803	0.16918200	−0.66747006
		0.6	0.54217805	0.19789280	−0.49067770
		1.2	0.50948539	0.20874837	−0.39272568
		1.8	0.48442692	0.21356226	−0.32816706
	0.5	0.0	0.62230372	0.13020184	−0.85400191
		0.6	0.58165832	0.17476862	−0.63901076
		1.2	0.55093356	0.19403963	−0.51974824
		1.8	0.52648523	0.20395391	−0.44110871
	2.0	0.0	0.67185164	0.03616084	−1.23522076
		0.6	0.64025457	0.10762118	−0.95764560
		1.2	0.61516518	0.14412953	−0.79794177
		1.8	0.59422219	0.16588697	−0.69078348
1.3	0	0.0	0.69419553	0.16472204	−0.89422492
		0.6	0.64319794	0.20488527	−0.67174008
		1.2	0.60489880	0.22057361	−0.54807678
		1.8	0.57466019	0.22757977	−0.46658107
	0.5	0.0	0.73182104	0.11210009	−1.12734182
		0.6	0.68774242	0.17232704	−0.85850372
		1.2	0.65323279	0.19935278	−0.70840723
		1.8	0.62497537	0.21359235	−0.60917368
	2.0	0.0	0.78345160	−0.01058070	−1.59864531
		0.6	0.75070112	0.08172075	−1.25623999
		1.2	0.72413662	0.13023044	−1.05758191
		1.8	0.70150511	0.15982364	−0.92353929

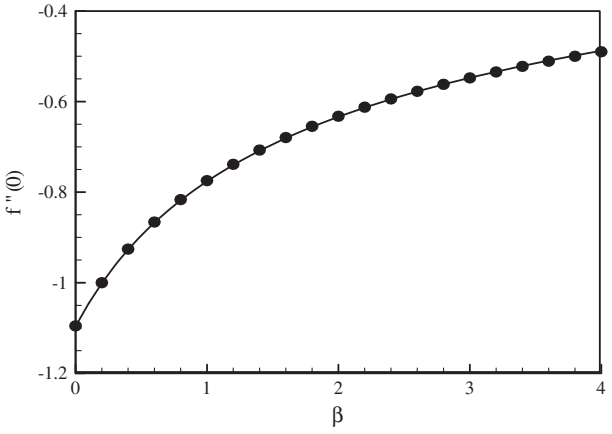

Figure 1 Variation of $f''(0)$ with Deborah number β for $\lambda = 0.2$; solid line: numerical solution; black circles: exact solution.

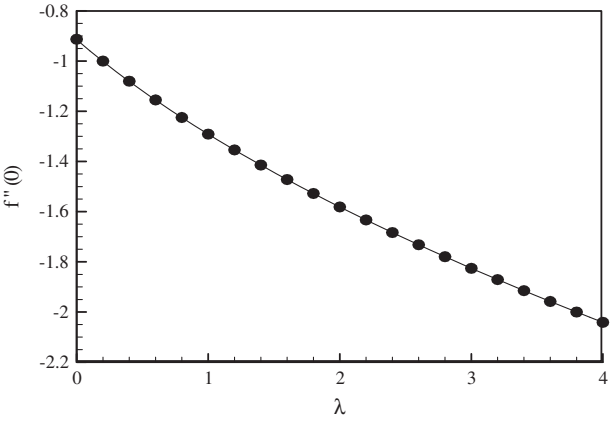

Figure 2 Variation of $f''(0)$ with λ for $\beta = 0.2$; solid line: numerical solution; black circles: exact solution.

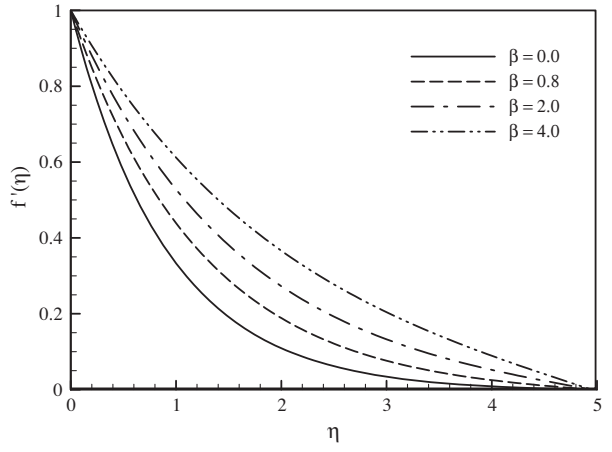

Figure 3 Dimensionless velocity profiles $f'(\eta)$ for various values of Deborah number β; $\lambda = 0.2$.

temperature is seen to be somewhat unaffected by the ratio of relaxation to retardation times λ particularly in the neighborhood of the sheet surface (i.e. $\eta = 0$). Nevertheless, further

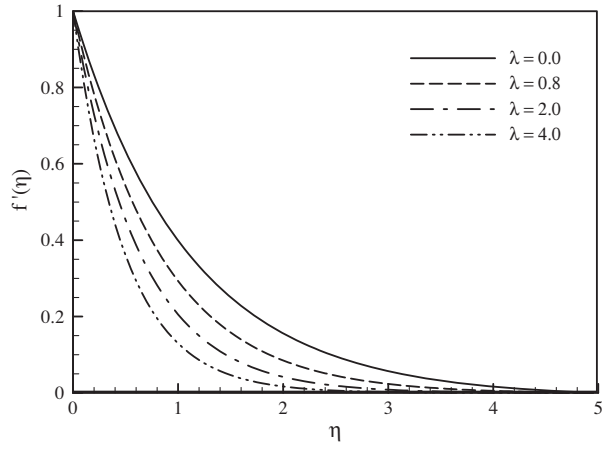

Figure 4 Dimensionless velocity profiles $f'(\eta)$ for various values of ratio of relaxation to retardation times λ; $\beta = 0.2$.

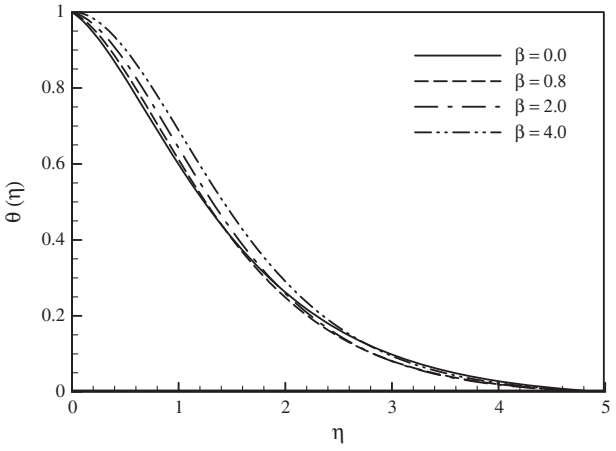

Figure 5 Dimensionless temperature profiles $\theta(\eta)$ for various values of Deborah number β; $\lambda = 0.2$, $Ec = 1.0$, $Pr = 1.0$.

away from the sheet inside the boundary layer, λ has a small effect on temperature, such that the temperature slightly increases with the increase of λ.

The effect of variation of Eckert number on temperature profile is illustrated in Fig. 7 for $\beta = 0.2$, $\lambda = 0.2$, $Pr = 1.0$. It is viewed that the Ec variation vastly influences the fluid temperature inside the boundary layer such that the higher the Ec, the greater the temperature. It is also seen that, for Ec values higher than $Ec = 2$, the dimensional temperature at the close vicinity of sheet goes above the sheet surface temperature T_w. It is seen from its definition that the Eckert number is directly proportional to the square of stretching velocity of the sheet, $(u_w)^2$. Hence, an increase in Ec means a great increase in the stretching rate of the sheet, and thus a large augmentation in motion of fluid particles near the sheet, which in effect increases the temperature of the fluid, especially at the sheet close vicinity. Fig. 8 shows the temperature profiles $\theta(\eta)$ for various values of Pr in $\beta = 0.2$, $\lambda = 0.2$, $Ec = 1.0$. It can be observed that the increase of Prandtl number causes the fluid temperature to reduce, while the temperature reduction is more pronounced at distances further away from the sheet in the boundary layer domain. An increase in Pr is equivalent

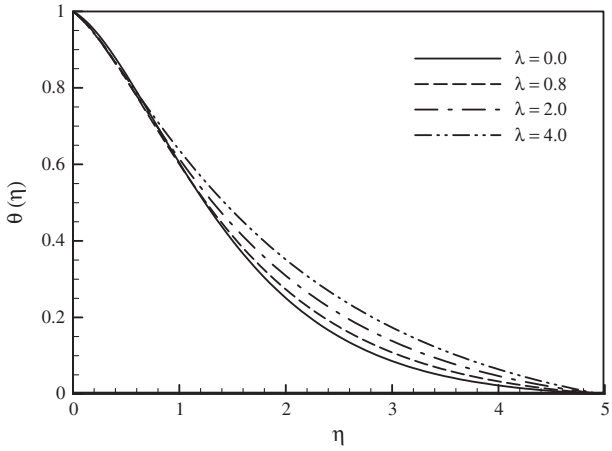

Figure 6 Dimensionless temperature profiles $\theta(\eta)$ for various values of ratio of relaxation to retardation times λ; $\beta = 0.2$, $Ec = 1.0$, $Pr = 1.0$.

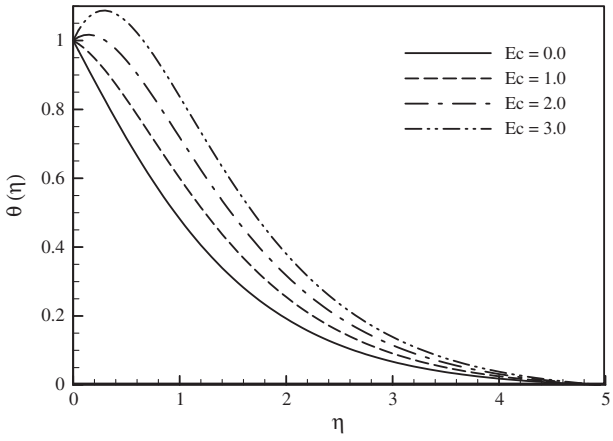

Figure 7 Dimensionless temperature profiles $\theta(\eta)$ for various values of Eckert number Ec; $\beta = 0.2$, $\lambda = 0.2$, $Pr = 1.0$.

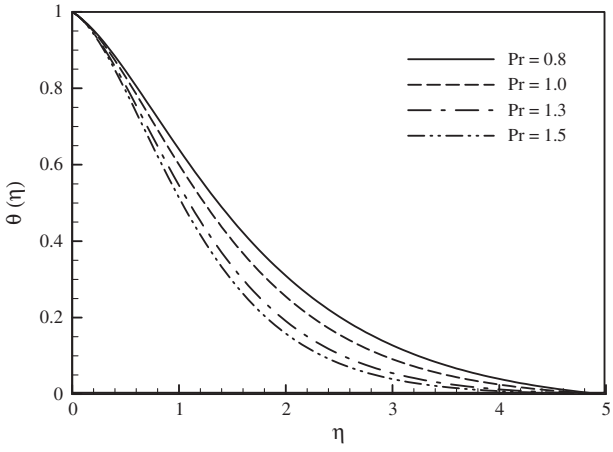

Figure 8 Dimensionless temperature profiles $\theta(\eta)$ for various values of Prandtl number Pr; $\beta = 0.2$, $\lambda = 0.2$, $Ec = 1.0$.

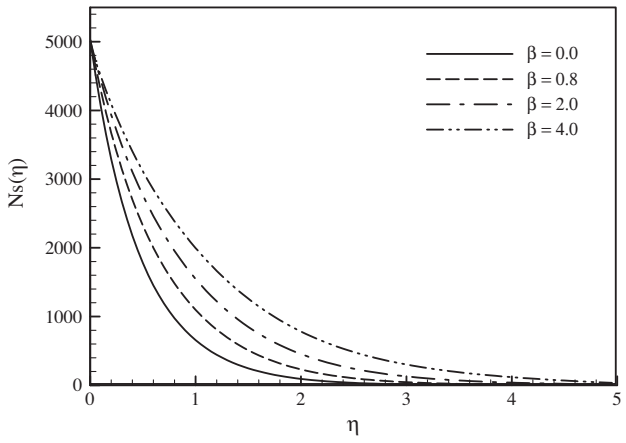

Figure 9 Dimensionless entropy generation number profiles $N_S(\eta)$ for various values of Deborah number β; $\lambda = 0.2$, $Ec = 1.0$, $Pr = 1.0$, $Re = 500$, $Br\Omega^{-1} = 10$.

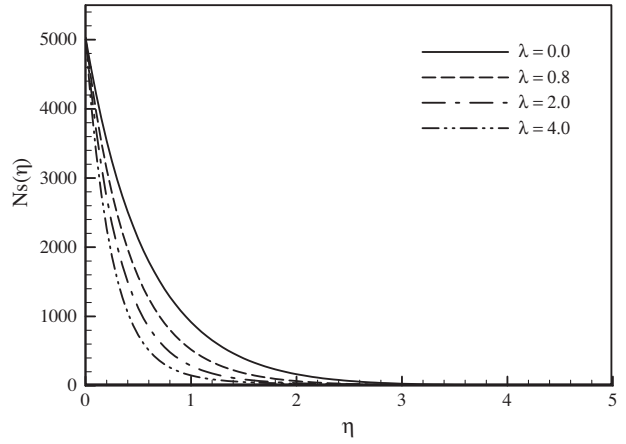

Figure 10 Dimensionless entropy generation number profiles $N_S(\eta)$ for various values of ratio of relaxation to retardation times λ; $\beta = 0.2$, $Ec = 1.0$, $Pr = 1.0$, $Re = 500$, $Br\Omega^{-1} = 10$.

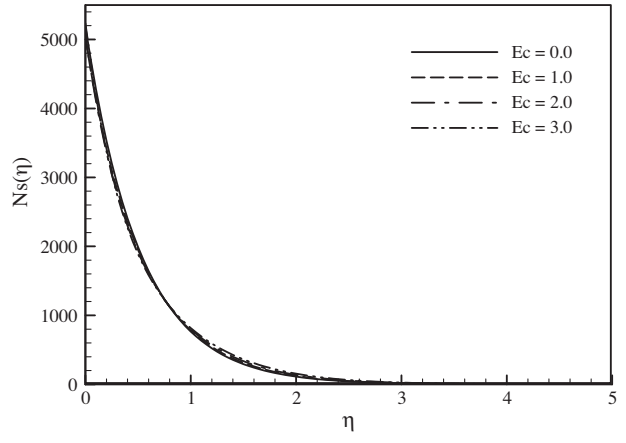

Figure 11 Dimensionless entropy generation number profiles $N_S(\eta)$ for various values of Eckert number Ec; $\beta = 0.2$, $\lambda = 0.2$, $Pr = 1.0$, $Re = 500$, $Br\Omega^{-1} = 10$.

with a decrease in the thermal diffusion of fluid layers resulting in a thinner thermal boundary layer and lower temperature.

Fig. 9 shows the dimensionless entropy generation number profiles $N_S(\eta)$ for various values of Deborah number β, when $\lambda = 0.2$, $Ec = 1.0$, $Pr = 1.0$, $Re = 500$, $Br\Omega^{-1} = 10$. It is revealed that the increase of Deborah number causes the dimensionless entropy generation number to boost. The reason is that the increase of Deborah number leads to higher motion of fluid particles inside the boundary layer. Higher motion of fluid particles itself can significantly increase the thickness of velocity boundary layer and so elevate fluid velocity. Higher motion of fluid particles can also make the thermal boundary layer slightly thicker and consequently promote the temperature. Thus the accumulated effects of velocity and temperature due to the β augmentation cause the increase of the entropy generation number. Fig. 10 demonstrates the dimensionless entropy generation number profiles $N_S(\eta)$ for various values of λ, for $\beta = 0.2$, $Ec = 1.0$, $Pr = 1.0$, $Re = 500$, $Br\Omega^{-1} = 10$. It can be observed that higher values of λ lead to lower values of N_S. The increase of N_S with an increase in the ratio of relaxation to retardation times λ is due to the fact that the velocity inside the boundary layer increases with an increase in λ, as observed in Fig. 4. However, it should be mentioned that a very low reduction in temperature with the increase of λ (Fig. 6) is not able to neutralize the velocity effect, and hence the entropy generation number increases.

Fig. 11 indicates $N_S(\eta)$ profiles for various values of Eckert number when $\beta = 0.2$, $\lambda = 0.2$, $Pr = 1.0$, $Re = 500$, $Br\Omega^{-1} = 10$. It is seen that the entropy generation number is slightly higher for larger values of Eckert number in distances far enough from the sheet in the boundary layer domain. This result is due to the effect of Eckert number on temperature (Fig. 7) in which the increase of Eckert number leads to the increase of temperature gradients. However, it can be said that the variation of Ec does not considerably influence N_S. For instance, when the Eckert number increases from 1.0 to 2.0, entropy generation number rises from the value of 780.85 to 797.66 which is a 2.15% increase in N_S for 100% increase in Ec. The dimensionless entropy generation number profiles $N_S(\eta)$ for various values of Pr at $\beta = 0.2$, $\lambda = 0.2$, $Ec = 1.0$, $Re = 500$, $Br\Omega^{-1} = 10$ are shown in Fig. 12. It is observed that N_S presents a very small increase with the increase of Pr, for distances not very close to or not too far from the sheet in vertical direction. Nevertheless, it can be concluded that Prandtl number variations do not have much effect on the entropy generation number values. It is observed that the entropy generation number varies from 816.34 to 839.79 when the Prandtl number increases from 1.5 to 2. This is an increase of 8.5% in N_S due to an increase of 100% in Pr.

Fig. 13 illustrates entropy generation number profiles $N_S(\eta)$ for various values of Brinkman number Br while $\beta = 0.2$, $\lambda = 0.2$, $Ec = 1.0$, $Pr = 1.0$, $Re = 500$, $\Omega^{-1} = 10$. It should be mentioned that the Brinkman number determines the relative importance of viscous effect. It is seen that the higher the Br values, the higher the N_S, although this outcome is more observable in the sheet surface vicinity (i.e. $\eta < 1.5$). This augmentation in N_S with the Br increase is due to the fact that for higher values of Br, the entropy generation number due to the fluid friction is higher. It should also be noticed that the entropy generation effects are more prominent near the sheet surface. These effects reduce as the distance from the surface

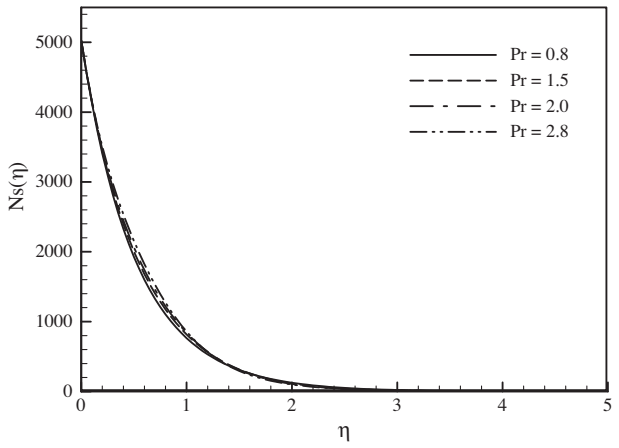

Figure 12 Dimensionless entropy generation number profiles $N_S(\eta)$ for various values of Prandtl number Pr; $\beta = 0.2$, $\lambda = 0.2$, $Ec = 1.0$, $Re = 500$, $Br\Omega^{-1} = 10$.

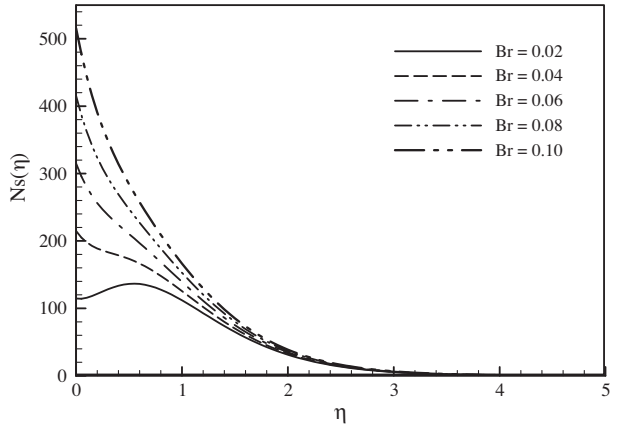

Figure 13 Dimensionless entropy generation number profiles $N_S(\eta)$ for various values of Brinkman number Br; $\beta = 0.2$, $\lambda = 0.2$, $Ec = 1.0$, $Pr = 1.0$, $Re = 500$, $\Omega^{-1} = 10$.

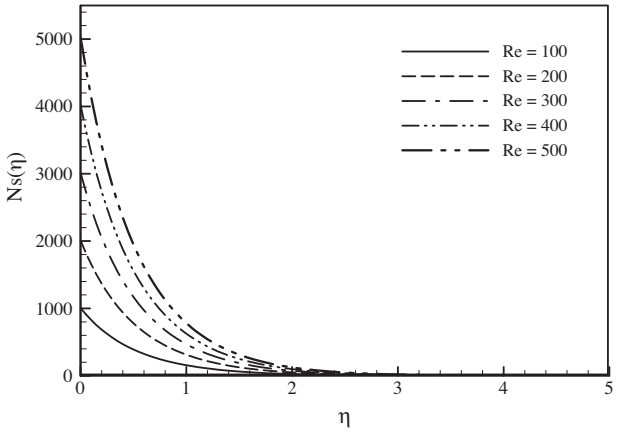

Figure 14 Dimensionless entropy generation number profiles $N_S(\eta)$ for various values of Reynolds number Re; $\beta = 0.2$, $\lambda = 0.2$, $Ec = 1.0$, $Pr = 1.0$, $Br\Omega^{-1} = 10$.

of the sheet increases. Since the Brinkman number is directly proportional to the square of sheet stretching velocity, on the surface of the sheet ($\eta = 0$) the dimensionless entropy generation number is higher for larger values of Br. The stretching velocity of the sheet also influences the fluid near the surface of sheet such that the fluid accelerates and the entropy generation number is increased. It can also be seen that for $Br \geqslant 0.04$ the N_S values decrease by getting further in distance from the sheet (i.e. increase of η). However, for $Br \leqslant 0.02$ with the increase of η the entropy generation number experiences an initial increase and then a slow reduction toward the distances far from the sheet.

In Fig. 14, the $N_S(\eta)$ profiles for various values of the Reynolds number when $\beta = 0.2$, $\lambda = 0.2$, $Ec = 1.0$, $Pr = 1.0$, $Br\Omega^{-1} = 10$ are given. It is seen that increasing the Reynolds number boosts the values of the entropy generation number. The increase of the Reynolds number augments the contribution of entropy generation number due to fluid friction and heat transfer inside the boundary layer. The reason is that the increase of the Reynolds number disturbs the fluid, and thus chaotic movements appear inside the fluid. With the increase of the Reynolds number, the inertia forces of the flow over the sheet are increased while the viscous forces are reduced. Hence, the fluid on the sheet is more accelerated and the resistance on the flow due to the sheet friction is diminished which consequently hoists the values of the entropy generation number. It is observed that the value of N_S at $\eta = 1$ increases from 156.17 to 780.86 when Re is increased from 100 to 500 which shows that the increase of Reynolds number by 100% causes the increase of entropy generation number by 80%. It can also be seen that with the increase of similarity variable (η) (i.e. going along the longitudinal direction of sheet) at a constant Reynolds number, the entropy generation number decreases monotonically.

6. Conclusions

The steady 2-D flow of a Jeffrey non-Newtonian incompressible fluid over a flat horizontal sheet is considered where the sheet is assumed to be an isothermal linearly stretching one. The boundary layer equations are transformed by using similarity transformations to two nonlinear ODEs and then solved using a numerical technique called Keller's box. The effects of various flow and thermal parameters, namely, Deborah number, ratio of relaxation time to retardation time, Prandtl number, Brinkman number and Reynolds number on velocity, temperature and entropy generation number are investigated. The results obtained are as follows:

(1) The dimensionless fluid velocity inside the boundary layer boosts with the increase of the Deborah number, while with the increase of the ratio of relaxation to retardation times the dimensionless fluid velocity reduces.
(2) With the increase of both Deborah number and the ratio of relaxation to retardation times, the dimensionless temperature of fluid inside thermal boundary layer slightly increases.
(3) The entropy generation number increases with the increase of Deborah number. However, the entropy generation number reduces with the increase of the ratio of relaxation to retardation times.

(4) Both the increase in Brinkman number and the increase in Reynolds number cause the increase of entropy generation number, and this increase in entropy generation number is more pronounced in adjacent of the sheet surface.

References

[1] M.M. Molla, L.S. Yao, Mixed convection of non-Newtonian fluids along a heated vertical flat plate, Int. J. Heat Mass Transfer 52 (2009) 3266–3271.

[2] T. Hayat, R. Sajjad, S. Asghar, Series solution for MHD channel flow of a Jeffery fluid, Commun. Nonlinear Sci. Numer. Simul. 15 (2010) 2400–2406.

[3] B. Sahoo, Flow and heat transfer of a non-Newtonian fluid past a stretching sheet with partial slip, Commun. Nonlinear Sci. Numer. Simul. 15 (2010) 602–615.

[4] K.V. Prasad, P.S. Datti, K. Vajravelu, Hydromagnetic flow and heat transfer of a non-Newtonian power law fluid over a vertical stretching sheet, Int. J. Heat Mass Transfer 53 (2010) 879–888.

[5] T. Hayat, M. Awais, S. Obaidat, Three-dimensional flow of a Jeffery fluid over a linearly stretching sheet, Commun. Nonlinear Sci. Numer. Simul. 17 (2012) 699–707.

[6] T. Hayat, Z. Iqbal, M. Mustafa, A. Alsaedi, Unsteady flow and heat transfer of Jeffrey fluid over a stretching sheet, Thermal Science (2012), http://dx.doi.org/10.2298/TSCI110907092H.

[7] Y. Khan, A. Hussain, N. Faraz, Unsteady linear viscoelastic fluid model over a stretching/shrinking sheet in the region of stagnation point flows, Sci. Iran. B 19 (6) (2012) 1541–1549.

[8] M.Y. Malik, I. Zehra, S. Nadeem, Numerical treatment of Jeffrey fluid with pressure-dependent viscosity, Int. J. Numer. Meth. Fluids 68 (2012) 196–209.

[9] T. Hayat, S.A. Shehzad, M. Qasim, S. Obaidat, Radiative flow of Jeffery fluid in a porous medium with power law heat flux and heat source, Nucl. Eng. Des. 243 (2012) 15–19.

[10] T. Hayat, S. Asad, M. Qasim, A.A. Hendi, Boundary layer flow of a Jeffrey fluid with convective boundary conditions, Int. J. Numer. Meth. Fluids 69 (2012) 1350–1362.

[11] M. Turkyilmazoglu, I. Pop, Exact analytical solutions for the flow and heat transfer near the stagnation point on a stretching/shrinking sheet in a Jeffrey fluid, Int. J. Heat Mass Transfer 57 (2013) 82–88.

[12] M. Goyal, R. Bhargava, Numerical solution of MHD viscoelastic nanofluid flow over a stretching sheet with partial slip and heat source/sink, ISRN Nanotechnol. (2013), doi: 1155/2013/931021.

[13] M. Qasim, Heat and mass transfer in a Jeffrey fluid over a stretching sheet with heat source/sink, Alexandria Eng. J. 52 (2013) 571–575.

[14] S. Nadeem, R.U. Haq, Z.H. Khan, Numerical solution of non-Newtonian nanofluid flow over a stretching sheet, Appl. Nanosci. 4 (2014) 625–631.

[15] S. Aiboud, S. Saouli, Entropy analysis for viscoelastic magnetohydrodynamic flow over a stretching surface, Int. J. Nonlinear Mech. 45 (2010) 482–489.

[16] O.D. Makinde, Second law analysis for variable viscosity hydromagnetic boundary layer flow with thermal radiation and Newtonian heating, Entropy 13 (2011) 1446–1464.

[17] M. Dehsara, M. Habibi-Matin, N. Dalir, Entropy analysis for MHD flow over a non-linear stretching inclined transparent plate embedded in a porous medium due to solar radiation, Mechanika 18 (5) (2012) 524–533.

[18] A.S. Butt, S.M. Unawar, A. Mehmood, A. Ali, Effect of viscoelasticity on entropy generation in a porous medium over a stretching plate, World Appl. Sci. J. 17 (4) (2012) 516–523.

[19] A.S. Butt, S. Munawar, A. Ali, A. Mehmood, Entropy generation in hydrodynamic slip flow over a vertical plate with convective boundary, J. Mech. Sci. Technol. 26 (9) (2012) 2977–2984.

[20] A. Malvandi, D.D. Ganji, F. Hedayati, M.H. Kaffash, M. Jamshidi, Series solution of entropy generation toward an isothermal flat plate, Therm. Sci. 16 (5) (2012) 1289–1295.

[21] N. Galanis, M.M. Rashidi, Entropy generation in non-Newtonian fluids due to heat and mass transfer in the entrance region of ducts, Heat Mass Transfer 48 (9) (2012) 1647–1662.

[22] A.S. Butt, S. Munawar, A. Ali, A. Mehmood, Entropy analysis of mixed convective magnetohydrodynamic flow of a viscoelastic fluid over a stretching sheet, Z. Naturforsch. A – J. Phys. Sci. 67 (8) (2012) 451–459.

[23] A.S. Butt, A. Ali, Entropy generation in MHD flow over a permeable stretching sheet embedded in a porous medium in the presence of viscous dissipation, Int. J. Exergy 13 (1) (2013) 85–101.

[24] A. Noghrehabadi, M.R. Saffarian, R. Pourrajab, M. Ghalambaz, Entropy analysis for nanofluid flow over a stretching sheet in the presence of heat generation/absorption and partial slip, J. Mech. Sci. Technol. 27 (3) (2013) 927–937.

[25] M. Dehsara, N. Dalir, M.R.H. Nobari, Numerical analysis of entropy generation in nanofluid flow over a transparent plate in porous medium in presence of solar radiation, viscous dissipation and variable magnetic field, J. Mech. Sci. Technol. 28 (5) (2014) 1819–1831.

[26] M.Z. Salleh, R. Nazar, N.M. Arifin, I. Pop, Numerical solutions of forced convection boundary layer flow on a horizontal circular cylinder with Newtonian heating, Malaysian J. Math. Sci. 5 (2) (2011) 161–184.